Simplifying the Kinematic Calibration of Parallel Mechanisms Using Vision-Based Metrology

Pierre Renaud, Nicolas Andreff, Jean-Marc Lavest, and Michel Dhome

***Abstract*—In this paper, a vision-based measuring device is proposed and experimentally demonstrated to be an accurate, flexible, and low-cost tool for the kinematic calibration of parallel mechanisms. The accuracy and ease of use of the proposed vision sensor are outlined, with the suppression of the need for an accurate calibration target, and adequacy to the kinematic calibration process is investigated. In particular, identifiability conditions with the use of such an exteroceptive sensor are derived, considering the calibration with inverse or implicit models. Extensive results are given, with the evaluation of the measuring device and the calibration of an H4 robot. Using the full-pose measurement, an experimental analysis of the optimal calibration model is achieved, with study of the kinematic behavior of the mechanism. The efficiency of the provided method is thus evaluated, and the applicability of vision-based measuring devices to the context of kinematic calibration of parallel mechanisms is discussed.**

***Index Terms*—Camera calibration, computer vision, kinematic calibration, metrology, parallel mechanisms.**

I. Introduction

PARALLEL mechanisms are emerging in the industry (e.g., machine tools, high-speed pick-and-place robots, flight simulators, medical robots). Indeed, these mechanisms have the main property of having their end-effectors connected with several kinematic chains to their base, rather than one for the standard serial mechanisms. This allows parallel mechanisms to bear higher loads, at higher speed and often with a higher repeatability [1]. However, their large number of links and passive joints often limits their performance in terms of accuracy [2]. A kinematic calibration is thus needed.

There exist several classes of methods to perform kinematic calibration of parallel mechanisms. The first one relies on the application of mechanical constraints on the end-effector or the mechanism legs [3], [4]. This class of methods is interesting, since it only needs joint measurements, but is hard to use in practice, since applying mechanical constraints accurately requires an accurate extra mechanism. Such methods also have the drawback of reducing the size of the workspace used for the calibration drastically, which significantly lowers the calibration sensitivity to the kinematic parameters, and therefore the calibration efficiency [5]. A second class of methods is known as self-calibration, and relies on the notion of redundant metrology. The underlying idea of such methods is to add extra proprioceptive sensors at the usually uninstrumented joints of the mechanism [6]–[9]. This allows for calibration in the whole available workspace, and only requires joint measurements. However, it is hard, in practice, to add these extra sensors on an existing mechanism, and sometimes almost impossible (think of a spherical joint).

The two remaining classes of methods rely on the kinematic models of the parallel mechanism, giving a nonlinear input–output relationship between the actuated joint values and the end-effector pose. On the one hand, one can find methods based on the forward kinematic model that come directly from the serial mechanism calibration class of methods. They consist of minimizing a nonlinear error between a measure of the end-effector pose and their corresponding values, estimated from the measured joint values through the forward kinematic model [10]–[12]. Their main advantage is that they can use whatever 3-D information is available, for instance, either only the position of the end-effector, or both its position and orientation. However, they suffer from a huge drawback, due to the absence in the general case of an analytical forward kinematic model. Hence, one must use a numerical estimation of it in the minimization of the nonlinear error, which may lead to numerical unstabilities [4].

On the other hand, for parallel mechanisms, the inverse kinematic model can usually be easily derived [1]. Therefore, the most natural method to perform calibration of a parallel mechanism is to minimize an error between the measured joint variables and their corresponding values, estimated from the measured end-effector pose through the inverse kinematic model [13], [14]. This method seems indeed to be the most numerically efficient among the calibration algorithms for parallel structures [5]. Nevertheless, it is constrained by the need for accurate measurement of the full end-effector pose (i.e., both its position and orientation). Some adapted measuring devices have been proposed (e.g., laser tracking systems [15], [16] or mechanical devices [17], [18]) that are either expensive or limitative as far as workspace is concerned.

Vision has been proposed for the kinematic calibration of serial mechanisms [19]–[21]. It enables one to achieve the needed full-pose measurement, with a low-cost sensor. Vision

Manuscript received October 27, 2004; revised April 29, 2005. This paper was recommended for publication by Associate Editor D. Prattichizzo and Editor S. Hutchinson upon evaluation of the reviewers' comments. This work was supported in part by the MAX project of the CNRS ROBEA program and in part by Région d'Auvergne.

P. Renaud was jointly with the LaMI, CNRS, Université Blaise Pascal, 63175 Aubière, France, and the LASMEA, CNRS, Université Blaise Pascal, 63177 Aubière, France. He is now with the INSA Strasbourg, 67084 Strasbourg, France (e-mail: Pierre.Renaud@insa-strasbourg.fr).

N. Andreff is with the LaMI, CNRS, Université Blaise Pascal, IFMA, 63175 Aubière, France, and also with the LASMEA, CNRS, Université Blaise Pascal, 63177 Aubière, France (e-mail: Nicolas.Andreff@ifma.fr).

J.-M. Lavest and M. Dhome are with the LASMEA, CNRS, Université Blaise Pascal, 63177 Aubière, France (e-mail: lavest@lasmea.univ-bpclermont.fr; dhome@lasmea.univ-bpclermont.fr).

Digital Object Identifier 10.1109/TRO.2005.861482

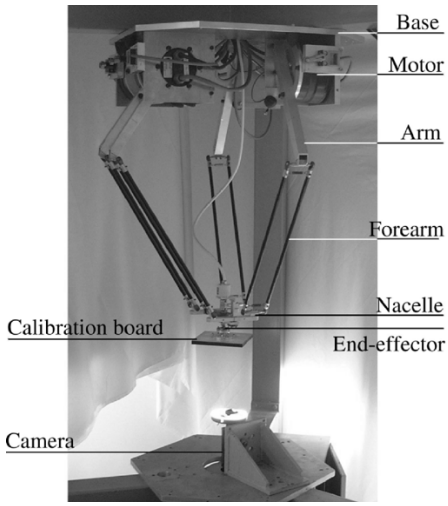

Fig. 1. Typical setup for vision-based calibration of a parallel mechanism; the H4 mechanism [25] and the vision-based measuring device.

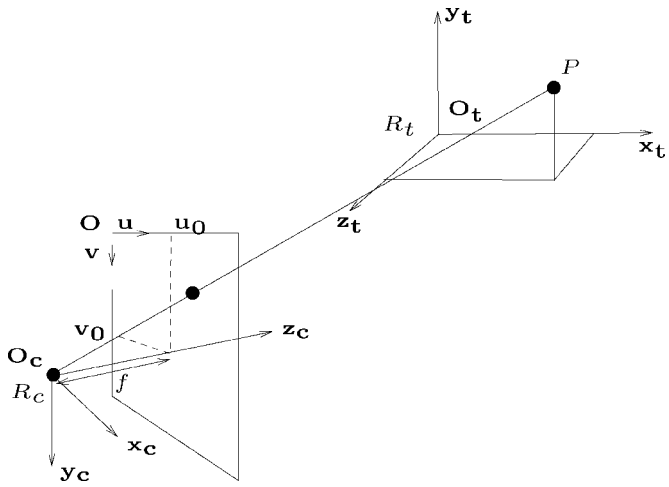

Fig. 2. Pinhole camera model, image geometry, and coordinate systems.

has, hence, been considered as a potential tool for kinematic calibration of parallel mechanisms [22], and evaluated with a commercial system [23] which remains high cost, and needs a three-camera system. In this paper, vision-based metrology is demonstrated to be the key for a low-cost flexible kinematic calibration method of parallel mechanisms. A monocular high-accuracy vision-based measuring device is introduced (Fig. 1), and classical calibration methods using the inverse or implicit kinematic models [7], [24] are used, with special attention given to the identifiability conditions due to the use of the vision-based sensor. Measurement accuracy is experimentally evaluated and calibration of an H4 robot [25] is achieved, with the analysis of the model's influence on the calibration efficiency. The accuracy improvement is hence demonstrated, and guidelines are provided on the applicability of the method.

The remainder of this paper is the following. In Section II, we propose the use of a low-cost, easy to use vision-based pose measurement, outlining the flexibility obtained by the simultaneous calibration of the camera and calibration target parameters. In Section III, we recall the calibration scheme, with specific insight on the fact that vision is used. In particular, we point out identifiability properties. Then, in Section IV, we evaluate the vision-based metrology accuracy by comparison with laser interferometry, and we apply the comprehensive calibration method to the H4 robot [25] designed at the Montpellier Laboratory of Computer Science, Robotics, and Microelectronics (LIRMM), Montpellier, France. A specific insight on the robot kinematic behavior is given with analysis of the optimal calibration model. Some concluding remarks are given in Section V on the efficiency of the proposed vision-based calibration scheme.

II. Vision-Based Metrology

A. Overview

Video cameras are becoming widely used for 3-D measurements. The use of vision-based metrology allows calculating a set of 3-D point coordinates (reconstruction) and/or to estimate the pose (position/orientation) of a known object (localization). Furthermore, a wide range of applications is concerned, as long focal lengths (i.e., zooming applications [26], [27]) as well as very short ones (3.5-mm fish-eye) may be used to obtain various inspection fields.

To obtain accurate results, the camera calibration problem needs to be solved. Calibration is necessary in order to determine the intrinsic parameters modeling the camera system. Well-known calibration techniques exist [28]–[30] that usually require a 3-D known object, called the *calibration target*. This object has to be well defined and accurately measured to ensure a reliable estimation of the camera parameters. The calibration technique used in this paper is based on former work [31] that demonstrated that camera calibration no longer requires an accurate calibration target, and hence, enables us to propose vision-based metrology as a flexible tool for the calibration of parallel mechanisms.

In this section, we outline the particularity of the developed vision-based pose measurement. After introduction of the classical modeling of the camera, including optical distortions, we derive the expressions of the multiview calibration approach that allows simultaneously obtaining accurate camera intrinsic parameters, the calibration target geometry, and their relative localization. This approach is known in computer vision as the *bundle adjustment technique* [32].

B. Definitions

A simplified camera model is used, i.e., the *pinhole* model, as depicted in Fig. 2. Through the paper, the following notations are used.

- $R_t(\mathbf{O_t}, \mathbf{x_t}, \mathbf{y_t}, \mathbf{z_t})$ is a right-handed 3-D coordinate system defining the world reference coordinate system, attached to the calibration target.
- $(\mathbf{O}, \mathbf{u}, \mathbf{v})$ is the 2-D image pixel system with its origin at the top-left corner of the image.
- $R_c(\mathbf{O_c}, \mathbf{x_c}, \mathbf{y_c}, \mathbf{z_c})$ is the 3-D camera coordinate system with its origin at the optical center $\mathbf{O_c}$, the $\mathbf{z_c}$ axis coincident with the optical axis, and $(\mathbf{x_c}, \mathbf{y_c})$ parallel to $(\mathbf{u}, \mathbf{v})$.

A transformation between two frames R_i and R_j is noted, ${}^i\mathbf{T}_j$. It is composed of the translation vector ${}^i\mathbf{t_j}$ and the rotation matrix ${}^i\mathbf{R}_j$. The vector ${}^i\mathbf{t_j}$ is defined by its three components

(x_{ij}, y_{ij}, z_{ij}), and the rotation matrix by the Bryant angles $(\alpha_{ij}, \beta_{ij}, \gamma_{ij})$.

The intrinsic parameters to be calibrated are the principal point (u_0, v_0) (Fig. 2), the focal length f, the pixel size of the charge-coupled device (CCD) array or its aspect ratio, and the distortion parameters of the optical system.

The components of the pose ${}^c\mathbf{T}_t$ of the target with respect to the camera, the so-called extrinsic parameters, have to be estimated simultaneously with the intrinsic parameters.

C. Classical Camera Calibration

We assume a perspective projection between a 3-D object point and its 2-D image. The relationship between the ith 3-D point and its 2-D image is described by the following equations:

$$\begin{pmatrix} x_i \\ y_i \\ z_i \end{pmatrix} = \lambda_i \left[{}^c\mathbf{R}_t \begin{pmatrix} X_i \\ Y_i \\ Z_i \end{pmatrix} + {}^c\mathbf{t}_t \right] \tag{1}$$

where (x_i, y_i, z_i) are the image-point coordinates in the camera frame R_c as defined in Fig. 2, and $z_i \equiv f$, i.e., the focal length of the camera, λ_i is a scale factor which maps a point in the camera coordinate system to the image plane, (X_i, Y_i, Z_i) are the object-point coordinates in the world-coordinate system R_t. Using the notations introduced in Section II-B, the translation vector ${}^c\mathbf{t_t}$ is defined by its three components (x_{ct}, y_{ct}, z_{ct}), and the rotation matrix ${}^c\mathbf{R}_t = (r_{ij})_{i,j=1,\ldots,3}$ by the three angles $(\alpha_{ct}, \beta_{ct}, \gamma_{ct})$.

If we eliminate λ_i in (1), omit the subscript i, and transform the image-point coordinates (x, y) into the pixel coordinate system $(\mathbf{O}, \mathbf{u}, \mathbf{v})$, we get the following so-called *collinearity equations* in photogrammetry:

$$\begin{cases} x = (u + v_x - u_0)dx - do_x = f\frac{r_{11}X + r_{12}Y + r_{13}Z + x_{ct}}{r_{31}X + r_{32}Y + r_{33}Z + z_{ct}} \\ y = (v + v_y - v_0)dy - do_y = f\frac{r_{21}X + r_{22}Y + r_{23}Z + y_{ct}}{r_{31}X + r_{32}Y + r_{33}Z + z_{ct}} \end{cases} \tag{2}$$

where v_x, v_y are errors of the measurements x and y, i.e., corrections to the measurements so that they fit the function values. Two parameters (dx, dy) define the pixel dimensions. The lens distortion components (do_x, do_y) consist of two parts, the *radial* and *tangential* distortions, parametrized by polynomial models with, respectively, the coefficients (a_1, a_2, a_3) and (p_1, p_2) [33].

Expression (2) can be reformulated as

$$\begin{cases} u + v_x = u_0 + \frac{do_x}{dx} + \left(\frac{f}{dx}\right)\frac{r_{11}X + r_{12}Y + r_{13}Z + x_{ct}}{r_{31}X + r_{32}Y + r_{33}Z + z_{ct}} = P(\mathbf{\Phi}) \\ v + v_y = v_0 + \frac{do_y}{dy} + \left(\frac{f}{dy}\right)\frac{r_{21}X + r_{22}Y + r_{23}Z + y_{ct}}{r_{31}X + r_{32}Y + r_{33}Z + z_{ct}} = Q(\mathbf{\Phi}) \end{cases} \tag{3}$$

that can also be rewritten as

$$\begin{cases} v_x = P(\mathbf{\Phi}) - u \\ v_y = Q(\mathbf{\Phi}) - v \end{cases}. \tag{4}$$

As the perspective projection is always defined up to a scale factor, dx parameter value is set to one. Defining $f_x = f/d_x$ and $f_y = f/d_y$, the calibration parameters to be estimated have the following expression:

$$\mathbf{\Phi} = [u_0, v_0, a_1, a_2, a_3, p_1, p_2, f_x, f_y, x_{ct}, y_{ct}, z_{ct}, \alpha_{ct}, \beta_{ct}, \gamma_{ct}]^T.$$

The calibration problem is now equivalent to estimating the vector $\mathbf{\Phi}$ by minimizing for a total number of n points $\sum_{i=1}^{n}(v_{x_i}^2 + v_{y_i}^2)$.

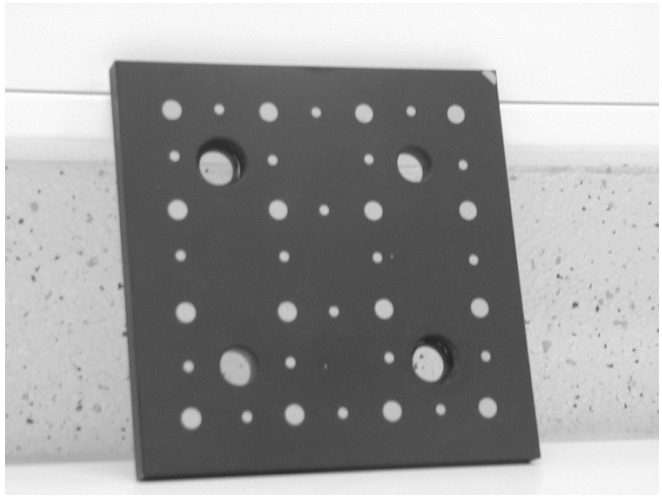

Fig. 3. View of a standard calibration target with 16 dots.

D. Suppressing the Need for Accurate Calibration Target

A major part of the calibration errors result from the measurement errors. These errors may come from the knowledge of the 3-D coordinates of the calibration target points, as well as the target point coordinates estimation in the image plane. It has been proved in [34] that subpixel accuracy measurements (2/100 pixel) can be obtained with special patterns like crosses or dots. In that case, the major source of calibration errors comes from the calibration pattern geometry knowledge. High-quality calibration patterns are difficult to achieve. They have to be mechanically stable in time (compared with the temperature change), or be moved very accurately to ensure an Euclidean reference frame without bias. Taking this point of view into consideration, we have proved [31] that it is possible to simultaneously estimate the intrinsic and extrinsic parameters, as well as the 3-D coordinates of the calibration target, using a multiple-images calibration approach. For a set of m images, the calibration task means computing the parameter vector

$$\begin{aligned} \mathbf{\Phi}_{9+6m+3n} = \Big[& u_0, v_0, a_1, a_2, a_3, p_1, p_2, f_x, f_y, \\ & X_1, Y_1, Z_1, \ldots, X_n, Y_n, Z_n, \\ & x_{ct}^1, y_{ct}^1, z_{ct}^1, \alpha_{ct}^1, \beta_{ct}^1, \gamma_{ct}^1, \ldots \\ & \ldots, x_{ct}^m, y_{ct}^m, z_{ct}^m, \alpha_{ct}^m, \beta_{ct}^m, \gamma_{ct}^m \Big]^T \end{aligned}$$

where n represents the total number of target points.

The total number of parameters to identify is then equal to

$$\begin{aligned} & 9 \text{ (intrinsic parameters)} + 3n \text{ (calibration point coordinates)} \\ & \qquad + 6m \text{ (extrinsic parameters)} \end{aligned}$$

while the number of equations is equal to $N = 2mn$. The redundancy of the system to be solved, $r = 2mn - (9 + 3n + 6m)$, can therefore be obtained easily: for a 16-point standard calibration pattern (Fig. 3) that is observed from 8 views, you get 256 measurements and 105 unknown parameters.

Notice that the numerical singularity when iterating over Bryant angles occurs when the calibration target is perpendicular to the image plane, i.e., in a physical configuration which is never reached.

Fig. 4. View of a typical eight-image calibration sequence of the vision-based measuring device.

E. Vision for Calibration

The accuracy of camera calibration proposed above relies on the use of several images and the relaxation of the known calibration target constraint. This implies, in return, the need for an extremely accurate point detection in the image. Thus, the algorithm requires a very careful implementation; however, it allows for high flexibility.

This flexibility is very useful for kinematic calibration, since a calibration target can be tailored at low cost to respect the constraints imposed by the mechanism. Then, before kinematic calibration can be started, some images of this calibration target are to be taken before its assembly to the end-effector for camera-plus-target calibration purposes. Simple empirical rules have to be respected: the calibration target has to be placed successively in the image corners, to be rotated around the optical axis and optionally around the other two axes (Fig. 4), so that the calibration target geometry, as well as the optical distortions, are correctly identified. About eight images are typically sufficient to get an accurate estimation of the parameters: the reprojection errors computed from (4) are then generally on the order of 2/100 pixel, which corresponds approximately to the estimation errors of the calibration target-dot centers. Finally, once this step is done, the pose of the target with respect to the camera can be obtained by solving (1) in ${}^c\mathbf{R}_t$ and ${}^c\mathbf{t_t}$ (see, for instance, [35]).

A drawback of vision-based measurements is the large amount of data from image collection that has to be treated. Using the approximate displacement value of the end-effector displacements determined from the *a priori* kinematic parameters, an automated image-detection procedure has been developed [36]. The overall procedure to get the pose measurement is hence accurate, and simultaneously simple and fast.

III. Kinematic Calibration

In this section, we give two alternate methods for calibrating a parallel mechanism using vision-based metrology. One is the classical method based on the inverse kinematic model, and the other is based on the implicit kinematic model. In both cases, we show that one must introduce additional parameters owing to the use of an exteroceptive measurement of the end-effector pose, and we consider the identifiability conditions, taking into account these parameters.

A. Calibration Using the Inverse Kinematic Model

Contrary to serial mechanisms, the inverse kinematic model of parallel mechanisms can often be expressed analytically [1]. It computes the joint variables $\mathbf{q}_c$ as a function of the end-effector pose ${}^b\mathbf{T}_e = ({}^b\mathbf{R}_e, {}^b\mathbf{t_e})$ with respect to the base frame and the kinematic parameter vector ξ_k. Zhuang *et al.* proposed [14] to form, for any pose ${}^b\mathbf{T}_{e_i}$, the following error:

$$\epsilon_i = \tilde{\mathbf{q}}_i - \mathbf{q}_c({}^b\tilde{\mathbf{T}}_{e_i}, \xi_k) \tag{5}$$

between the corresponding measured joint values $\tilde{\mathbf{q}}_i$ and the computed ones $\mathbf{q}_c({}^b\tilde{\mathbf{T}}_{e_i}, \xi_k)$, then to determine the kinematic parameters by measuring, with an exteroceptive sensor, m different poses ${}^b\tilde{\mathbf{T}}_{e_i}$, $i \in [1, m]$, and finally estimate ξ_k by the nonlinear minimization of the following cost function with respect to ξ_k:

$$\chi^2(\xi_k) = \epsilon^T\epsilon, \quad \epsilon = (\epsilon_1^T, \ldots, \epsilon_m^T)^T. \tag{6}$$

However, this suggests that the end-effector pose can be measured in the base frame. Due to the use of an exteroceptive measuring device, this, in fact, can not be achieved, since one shall take into account the pose of the measuring device with respect to the base frame ${}^b\mathbf{T}_c$, and, which is not evident, the pose of the target of the measuring device with respect to the end-effector ${}^e\mathbf{T}_t$. Indeed, any measuring device needs a target, which can be a reflective cube for a laser tracker system, reflective amers for a theodolite, or a physical interface part for a mechanical measuring machine. When using vision, the measuring device is composed of a fixed CCD camera and a target attached to the end-effector,[1] and gives the pose of the target with respect to the camera, as shown in Section II.

Formally, this implies that one measures poses of the target with respect to the measuring device ${}^c\mathbf{T}_{t_i}$, which are related to the end-effector poses with respect to the base by the unknown

[1]We could also think of using an on-board camera observing a fixed target, which only has for influence in the following to swap c and t in the superscripts and subscripts.

above-mentioned constant rigid transformations ${}^b\mathbf{T}_c$ and ${}^e\mathbf{T}_t = {}^t\mathbf{T}_e^{-1}$ through

$$ {}^b\mathbf{T}_{e_i} = {}^b\mathbf{T}_c\, {}^c\mathbf{T}_{t_i}\, {}^t\mathbf{T}_e \quad \forall i \in [1,m]. \tag{7}$$

Therefore, instead of the error in (5), one should use the following error:

$$ \epsilon_i = \tilde{\mathbf{q}}_i - \mathbf{q}_c({}^b\mathbf{T}_c\, {}^c\tilde{\mathbf{T}}_{t_i}\, {}^t\mathbf{T}_e, \xi_k). \tag{8}$$

Noting ξ_e the external parameters [37], i.e., the set of parameters describing ${}^b\mathbf{T}_c$ and ${}^t\mathbf{T}_e$, the problem of parallel-mechanism kinematic calibration based on the inverse kinematic model can be formally stated as the following nonlinear minimization problem:

$$ \min_{\xi_k,\xi_e} \sum_{i=1}^{m} ||\tilde{\mathbf{q}}_i - \mathbf{q}_c({}^c\tilde{\mathbf{T}}_{t_i}, \xi_k, \xi_e)||^2. \tag{9}$$

One may notice that these external parameters appear in each equation of the inverse kinematic model. Identification of all the mechanism legs must, hence, be *a priori* achieved simultaneously rather than independently.

B. Calibration Using the Implicit Kinematic Model

An alternate model of a parallel mechanism is the implicit kinematic model [7], [24], which expresses the closure of the kinematic chains. We do not know of a parallel mechanism which does not have an analytical formulation of these closure equations. Notice that usually, the inverse kinematic model is extracted by algebraic manipulation from the implicit kinematic model.

Formally, the implicit kinematic model is an equation relating the joint values, the end-effector pose, and the kinematic parameters. In the case we are dealing with, where the end-effector pose is measured, the implicit kinematic model takes the following generic expression:

$$ \Psi(\mathbf{q}, {}^c\mathbf{T}_t, \xi_k, \xi_e) = 0. \tag{10}$$

Then, the problem of parallel-mechanism kinematic calibration based on the implicit kinematic model can be formally stated as the following nonlinear minimization problem:

$$ \min_{\xi_k,\xi_e} \sum_{i=1}^{m} ||\Psi(\tilde{\mathbf{q}}_i, {}^c\tilde{\mathbf{T}}_{t_i}, \xi_k, \xi_e)||^2. \tag{11}$$

C. Identifiability

Calibrating a robot is an identification process, and hence, one should take a careful look at the identifiability of the model parameters, i.e., one should be able to answer the following questions.

- Can we estimate all the parameters in the model?
- If not, is it due to the set of poses chosen for the identification, or are there nonidentifiable parameters?
- If yes, are the poses selected for the identification optimal for the determination of the parameters?

The answers to those questions are related to the nonlinear minimization problem numerical solution. Most of the time, people use iterative algorithms (such as Newton, Gauss, or Levenberg–Marquardt) solving, at each iteration j, a linear least-square (LS) approximation of the cost function

$$ \frac{\partial \chi^2(\xi_j)}{\partial \xi}(\xi_{j+1} - \xi_j) = \chi^2(\xi_j) \tag{12}$$

where ξ_j is the jth estimation of the parameters $\xi = \xi_k \cup \xi_e$, and $\chi^2(\xi)$ is, in our case, given either by (9) or (11).

It is easy to understand that the estimation update step can only be done on the components of ξ that do not lie in the kernel of the regressor $\partial\chi^2(\xi_j)/\partial\xi$. A parameter which is in the kernel of the regressor at every iteration will not be identifiable, i.e., its value will not be updated from the *a priori* estimate. Therefore, much work was led on finding the so-called optimal excitation [38], [39], that is, the experiment which leads to the optimal estimation of the parameters. In the case of kinematic calibration, this boils down to the selection of an optimal set of robot configurations [40]–[42].

However, there can be a so-called structural loss of rank [37]. Indeed, the model can be such that whatever the excitation is, then the regressor is always rank-deficient. This means that there exist linearly dependent combinations between the columns of the regressor. Reminding that there is a one-to-one correspondence between the columns of the regressor and the parameters, one may define the set of base parameters, which is the largest set of parameters (or combinations thereof), such that their associated columns are linearly independent. In the context of serial mechanisms, analytical methods have been developed to determine the base parameters [43], [44]. In the context of parallel mechanisms, numerical estimation has been proposed [5]. We propose here a formal derivation of the identifiability conditions, to outline the consequences of the use of an exteroceptive sensor.

Omitting the iteration subscript, the regressor is thus of the form

$$ \frac{\partial \chi^2(\xi)}{\partial \xi} = \begin{pmatrix} \frac{\partial \chi^2(\xi)}{\partial \xi_k} & \frac{\partial \chi^2(\xi)}{\partial \xi_e} \end{pmatrix}. \tag{13}$$

Loss of rank can occur in three cases.

1) Nonidentifiable Kinematic Parameters: The kinematic parameters are identifiable if the model used for calibration is minimally parameterized. This only depends on the mechanism itself, and should have been checked already at the modeling stage.

Formally, if there exist nonidentifiable kinematic parameters, then there exists a full-rank matrix $\mathbf{A}_k$, a combination matrix $\mathbf{C}_k$ (possibly rank-deficient), and a permutation matrix $\mathbf{P}_k$ (i.e., $\mathbf{P}_k^2 = \mathbf{I}$) such that

$$ \frac{\partial \chi^2(\xi)}{\partial \xi_k} = \begin{pmatrix} \mathbf{A}_k & \mathbf{A}_k\mathbf{C}_k \end{pmatrix} \mathbf{P}_k. \tag{14}$$

Hence, we can reorder the parameter vector ξ_k with the permutation matrix $\mathbf{P}_k$ and then split the result in two parts: $(\mathbf{P}_k\xi_k)^T = (\xi_{k'}^T, \xi_{k_{\overline{id}}}^T)$, where $\xi_{k'}$ corresponds to the full-rank matrix $\mathbf{A}_k$ and $\xi_{k_{\overline{id}}}$ corresponds to the dependent part $\mathbf{A}_k\mathbf{C}_k$. The vector $\xi_{k_{\overline{id}}}$ contains the nonidentifiable kinematic parameters. They do not have any individual influence on the mechanism behavior, and generate columns in the regressor that uselessly make the latter singular. Therefore, $\xi_{k_{\overline{id}}}$ can be thrown away (i.e., set to an arbitrary value, which can be zero or an *a priori* value), and the base parameters are to be found in $\xi_{k'}$.

2) Nonidentifiable External Parameters: External parameters only appear in (7). Therefore, nonidentifiable external parameters are such that the end-effector pose with respect to the base is left unchanged if we modify them. Hence, they do not have any influence on the mechanism behavior. However, it is of importance to detect such nonidentifiable external parameters to suppress the corresponding columns in the regressor that also uselessly make the latter singular. This can be done similarly as for the kinematic parameters by writing

$$\frac{\partial \chi^2(\xi)}{\partial \xi_e} = \begin{pmatrix} \mathbf{A}_e & \mathbf{A}_e\mathbf{C}_e \end{pmatrix} \mathbf{P}_e \tag{15}$$

and splitting the external parameters in the nonidentifiable external parameters $\xi_{e_{\overline{id}}}$ and the remainder $\xi_{e\prime}$.

Notice that the loss of external parameters identifiability can be related to the number of degrees of *spatiality* of the mechanism [36].

3) Coupled Kinematic and External Parameters: From the previous two cases, we can rewrite (13) as

$$\frac{\partial \chi^2(\xi)}{\partial \xi} = \begin{pmatrix} \mathbf{A}_k & \mathbf{A}_e & \mathbf{A}_e\mathbf{C}_k & \mathbf{A}_e\mathbf{C}_e \end{pmatrix} \tag{16}$$

associated with the reordered parameter set $(\xi_{k\prime}^T, \xi_{e\prime}^T, \xi_{k_{\overline{id}}}^T, \xi_{e_{\overline{id}}}^T)^T$.

Now, although $\mathbf{A}_k$ and $\mathbf{A}_e$ have full rank, their compound $(\mathbf{A}_k\mathbf{A}_e)$ may be rank-deficient. Similar to the above two cases, we can split it in two parts: one full-rank matrix and one linearly dependent part. Thereby, we also reorder, then split, the vector $(\xi_{k\prime}^T, \xi_{e\prime}^T)^T$ in two parts: the vector containing the base parameters ξ_{base}, and a second part ξ_{coupled}, which contains the remaining parameters that can not be identified.

Remark 1: Notice that both parts may contain kinematic *and* external parameters. Therefore, ξ_{coupled} may contain a part defining the mechanism behavior and a part related to the measure of the end-effector pose, while together, these two parts do not appear in the error used for calibration. This means that if one removes the exteroceptive measuring device at control time, then there will be missing kinematic knowledge in the model, and therefore, the control will be inaccurate.

Remark 2: $\mathbf{A}_e$ is the partial derivative of the inverse (resp. implicit) model with respect to (w.r.t.) the external parameters, and each column $\mathbf{A}_{ei}$ can be expressed as

$$\mathbf{A}_{ei} = \mathbf{J}_{\mathbf{X}} \frac{\partial \mathbf{X}}{\partial \xi_{ei}} \tag{17}$$

with $\mathbf{X}$ the mechanism pose determined from ${}^b\mathbf{T}_e$, and $\mathbf{J}_{\mathbf{X}}$ the mechanism inverse Jacobian matrix. The existence of coupled kinematic and external parameters depends, therefore, on the mechanism inverse Jacobian matrix. Consequently, it is a tough problem to analytically determine such a coupling, since the analytical expression of the inverse Jacobian matrix is complex, and depends on the robot configurations. This differs from the case of serial robots, where such a coupling appears directly in the forward kinematic model and independently from the robot configuration.

If inverse Jacobian matrix rank loss occurs because of coupled kinematic and external parameters, a solution would be to turn to calibration methods without exteroceptive sensing, or to keep the exteroceptive measure at control time (for instance, to use visual-servoing techniques [45], [46]).

Fig. 5. Setup of the vision-based metrology evaluation. Left (fixed): an LCD target, a laser interferometer station, and its beam splitter block. Right (in motion): a CCD camera and the laser retroreflective block.

TABLE I
VISION-BASED METROLOGY AND LASER INTERFEROMETRY ACCURACIES (R_z NONMEASURABLE WITH LASER INTERFEROMETRY)

	$T_x(\mu m)$	$T_y(\mu m)$	$T_z(\mu m)$	$R_x(^\circ)$	$R_y(^\circ)$	$R_z(^\circ)$
Laser	1.15	1.15	0.35	1.7E-5	1.7E-5	
Vision	2.2	2.2	10.5	1.5E-3	1.5E-3	1.0E-3

IV. EXPERIMENTS

A. Vision-Based Metrology Evaluation

To experimentally evaluate the accuracy of the vision-based metrology, we compared it with laser interferometry (see [47] for a detailed analysis of the experimental procedure). To do so, we used a high-speed machine-tool axis to perform accurate linear motions (Fig. 5).

Notice that while vision gives a full Cartesian pose (i.e., six values), laser interferometry can only give one scalar measure at a time, and one needs to change the optical blocks (beam splitter and retroreflective) to pass from one measure to another. Hence, one can not consider that the measures from laser interferometry are obtained in the same frame. Moreover, the laser gives a displacement, while vision gives an absolute position. For comparison, a set of displacements is then imposed on the machine-tool axis, and standard deviation of the errors between imposed displacements and measurements, from vision or interferometry, is computed.

We used a 1024×768 CCD camera with a 3.6-mm focal lens and a Renishaw ML-10 interferometer. The estimated standard deviations are given in Table I. The largest measurement errors concern the translation along the optical axis and rotations in the perpendicular directions, which is due to the use of a monocular system. Nevertheless, vision-based metrology yields a competitive accuracy, compared with interferometry.

B. Calibration of the H4 Robot

The comprehensive calibration method is now applied to the H4 robot with the experimental setup displayed in Fig. 1. This implies the modeling of the mechanism, its identifiability analysis, the identification of the parameters using the collected experimental data, and validation tests. We present here these four steps.

The H4 robot has four degrees of mobility (three translations plus one rotation around the vertical axis), provided that the

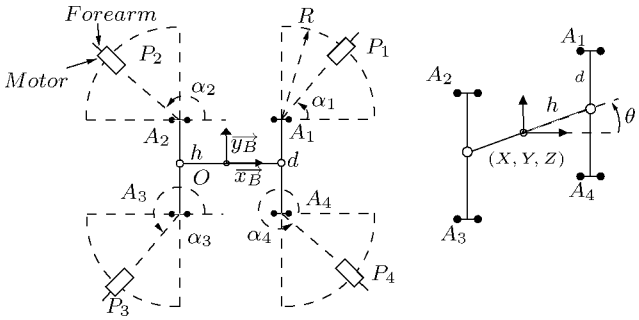

Fig. 6. CAD model of the H4 robot. Top view for the joint parameter definitions (left) and nacelle scheme (right).

four-bar mechanisms in the arms are articulated parallelograms. This assumption is considered valid, and will be verified with the experimental results.

1) Kinematic Models: Different models of the robot can be obtained, depending on which hypotheses considered during the mechanism design are used. Taking into account all these hypotheses, the model of the H4 robot gives the following implicit model (see [25] for a detailed expression), expressing the closure of the kinematic chain around each leg, under the hypothesis of the existence of some symmetries in the mechanism (Fig. 6):

$$\begin{aligned} L^2 - l^2 - \| \overrightarrow{P_iA_i} \|^2 = & -2\big(\overrightarrow{P_iA}_{ix}.l.\cos(\alpha_i).\cos(q_i - q_{0_i}) \\ & + \overrightarrow{P_iA}_{iy}.l.\sin(\alpha_i).\cos(q_i - q_{0_i}) \\ & - \overrightarrow{P_iA}_{iz}.l.\sin(q_i - q_{0_i})\big) \end{aligned} \tag{18}$$

with L the arm length, l the forearm length (both the same for each leg), q_{0_i} the encoder offsets, and other notation given in Fig. 6. Notice that the A_i's depend on the end-effector pose, denoted by (X, Y, Z, θ), with θ the end-effector angle such that $\theta = 0$ when the nacelle has an "H" shape. The nacelle dimension d does not appear in this model.

This implicit kinematic model is parameterized by 12 scalars: $(R, l, L, h, \alpha_i, q_{0_i})$, $i \in [1, 4]$ and will be referred to as the *implicit 12-model* in the following.

From this model, one can derive rather easily its inverse kinematic model (the so-called *inverse 12-model*)

$$q_i = q_{0_i} + 2\arctan\left(\frac{N_i + \epsilon_i\sqrt{N_i^2 + M_i^2 - G_i^2}}{G_i + M_i}\right), i \in [1, 4] \tag{19}$$

with $M_i = -2l(\overrightarrow{P_iA}_{ix}\cos\alpha_i + \overrightarrow{P_iA}_{iy}\sin\alpha_i)$, $N_i = 2l\overrightarrow{P_iA}_{iz}$, $G_i = L^2 - l^2 - \| \overrightarrow{P_iA_i} \|^2$, and $\epsilon_i = \pm 1$ depending on the assembly.

A more general kinematic model can be used. The base frame is then attached to the first joint center P_1 and its axis $\vec{z}_b$ parallel to the end-effector rotation axis. Like the 12-model, the base-frame orientation is such that θ is the angle between the "H-configuration" of the nacelle and its current configuration. The other joints can be placed at any point $P_i = (x_i, y_i, z_i)$, $i \in [2, 4]$. Each joint may have any orientation (β_i, ψ_i), $i \in [1, 4]$, and the legs have independent arm and forearm lengths (L_i, l_i), $i \in [1, 4]$. Thus, this *implicit 31-model* involves a total of 31 parameters $(x_i, y_i, z_i, \beta_j, \psi_j, q_{0_j}, l_j, L_j, h, d)$, $i \in [2, 4], j \in [1, 4]$ and becomes rather complicated

$$\| L_i \vec{V}_i + \vec{W}_i \|^2 = {l_i}^2 \tag{20}$$

with

$$\begin{aligned} \vec{V}_i = & (\sin(q_i + q_{i0})\cos(\beta_i)\sin(\psi_i) - \cos(q_i + q_{i0})cos(\psi_i) \\ & - \sin(q_i + q_{i0})\cos(\beta_i)\cos(\psi_i) - \cos(q_i + q_{i0})\sin(\psi_i) \\ & - \sin(q_i + q_{i0})\sin(\beta_i)) \\ \vec{W}_i = & \begin{pmatrix} X - x_i + (1 + \epsilon_{1i} - \epsilon_{1i}\cos(\theta))h \\ Y - y_i + d - \epsilon_{1i}h\sin(\theta) \\ Z - z_i \end{pmatrix}. \end{aligned}$$

The inverse model can be expressed in a similar way to the 12-model. Its expression is derived in [36].

2) Identifiability: The three sources of identification of Jacobian loss of rank are investigated for the two models. First, it can be noticed that the nacelle rotation axis is equal to the $\vec{z}_b$ base-frame vector for 12 and 31 models. The full-pose measurement enables us to then determine experimentally in a first step this vector in the camera frame. Using the notations introduced in Section II-B, only four parameters $(x_{bc}, y_{bc}, z_{bc}, \gamma_{bc})$ of the transformation ${}^b\mathbf{T}_c$ have then to be identified. The experimental setup is also designed in such a way that only the four external parameters $(x_{te}, y_{te}, z_{te}, \gamma_{te})$ are needed to define ${}^t\mathbf{T}_e$.

Kinematic Parameters: Computation of the condition number of the identification Jacobian matrix for the kinematic parameters shows that the 12-model and 31-model parameter sets are identifiable.

External Parameters: Analyzing the models shows that for both cases, the parameters z_{cb} and z_{te} defining, respectively, the position along the camera optical axis of the calibration target w.r.t. the end-effector, and the position of the base-frame center w.r.t. the camera can only be identified simultaneously. This is due to the fact that the end-effector only has one degree of freedom in rotation and can be related to results on hand–eye calibration [48].

External and Kinematic Parameters: Numerical estimation of the identification Jacobian matrix shows that no rank loss occurs when considering the complete set of parameters for the 12-model.

On the contrary, for the 31-model, the kinematic parameter d is coupled with the external parameter y_{bc}, a translation component of ${}^b\mathbf{T}_c$. Thus, only the *a priori* value of d can be used when needed. The consequence of this coupling between external and kinematic parameters is here a constant offset on the zero-reference point of the end-effector. This means that the displacements of the end-effector can be controlled, but a constant gap between the end-effector position in the base frame and its real position can remain in the $\vec{y}_B$ direction. Since a robot task is generally defined between a world frame and a tool frame, distinct from the base and end-effector frames, the problem of the determination of the zero-reference point of the end-effector is included in the calibration of the world/base and tool/end-effector transformations. The nonidentifiability of the parameter d can then be taken into account when estimating these transformations, at the task-planning stage (workpiece localization). In the same way, one can show [36] that a constant error remains

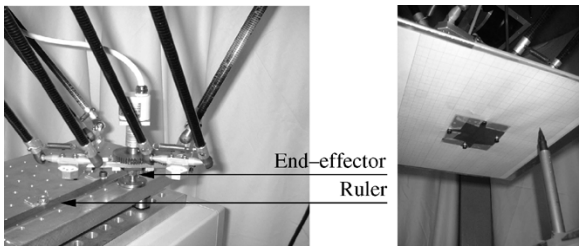

Fig. 7. Validation setup. Linearity check (left) and control validation (right).

in the nacelle configuration defined by the angle θ, due to a coupling between the kinematic and external parameters. Such an error can also be compensated for.

3) Identification From Collected Experimental Data: We collected in a first step eight images of the calibration target shown in Fig. 3, and used them for calibrating the measuring device, following the empirical rules given in Section II-E. Then, we moved the robot in 27 uniformly distributed positions in the workspace, and in each position, we rotated the nacelle in three different orientations ($-50°$, $0°$, $50°$), thus gathering 81 poses. In each pose, we recorded an image and the corresponding joint values. Finally, 71 out of these 81 poses were randomly chosen for the kinematic calibration.[2] The condition number of the kinematic parameters Jacobian is on the order of 150, which is quite satisfactory [49], but could have been improved by a pose-optimization procedure [41].

The kinematic parameters are then identified from the error function (9) and (11), using a Levenberg–Marquardt method with computed Jacobian matrices.

4) Validation: Three validation procedures have been used to validate the calibration efficiency. First, with the 10 unused poses, we computed the mean and root mean square (RMS) error between the measured joint variables and their estimated value obtained with the identified inverse kinematic model. Since the vision-based measuring device is used to obtain the validation data, this test is not completely independent from the calibration procedure. It allows one, however, to evaluate the absolute accuracy obtained after calibration, i.e., the errors between a controlled pose defined between the base frame and the end-effector frame and the corresponding measured location. One must notice that the base frame can not physically be used for validation tests due to its definition. The other two tests are, therefore, based on the evaluation of the relative accuracy, i.e., accuracy of the end-effector displacements, and provide independent validation data.

The second validation test is based on a kinematic constraint applied to the end-effector (Fig. 7). A linearity check has been achieved in three steps:

1) the end-effector was manually moved along a straight ruler while recording the joint values in several stations;
2) we applied a numerical estimation of the forward kinematic model to the joint values in each position with the estimated kinematic parameters. This gave us an estimation of each of the end-effector poses, from which we computed an LS estimate of the straight line they are constrained to lie on;
3) we computed the standard deviation with respect to the mean straight line.

The accuracy of this second test is on the order of 0.05 mm.

The third validation test is based on a control validation, using the inverse 12-model. Indeed, using the Cartesian control mode of the robot, we required the end-effector to move to the 4 corners of a 100-mm square, twice with the *a priori* values of the parameters obtained from the mechanism design to check the robot repeatability, and once with the estimated parameters (Fig. 7). The distances between the four corners is graphically measured with an accuracy on the order of 0.5 mm.

5) Results: In Table II, we give the *a priori* and identified values of the kinematic parameters for the 12-model.[3] The residual validation tests are given in Table III, and the linearity check along two approximately orthogonal directions in Table IV. For the inverse 12-model, Fig. 8 shows the results of the validation by control. One can see two parallel trajectories obtained with *a priori* kinematic parameters for two different positions of the pen that validate the repeatability of the robot. One can, more interestingly, see a third trajectory obtained after calibration. The error is reduced from about 1 cm down to 1 mm, which is on the order of the validation test uncertainties.

TABLE II
A PRIORI AND IDENTIFIED KINEMATIC PARAMETERS FOR THE 12-MODEL

	Model	*a priori*	implicit 12	inverse 12
Dimensions	h (mm)	60	61	61
	L (mm)	480	488.6	487.2
	l (mm)	260	259.8	259.6
Joint positions	R (mm)	140	140.3	141.1
	α_1 (°)	0	-2.9	0.1
	α_2 (°)	180	175.9	177.3
	α_3 (°)	270	268.0	267.8
	α_4 (°)	270	268.2	268.1
Joint offsets	q_1 (°)	0	-3.7	-3.9
	q_2 (°)	0	-0.4	-1.1
	q_3 (°)	0	-2.8	-3.0
	q_4 (°)	0	-3.2	-3.5

TABLE III
RESIDUAL TEST (IN DEGREES)

Joint variable	q_1	q_2	q_3	q_4
a priori parameters				
Mean error	5.1	0.2	4.2	4.7
RMS error	5.1	2.1	4.2	4.7
implicit 12-model				
Mean error	-4.6e-3	-2.8e-3	-5.7e-3	-1.1e-3
RMS error	6.3e-2	6.9e-2	6.3e-2	6.3e-3
inverse 12-model				
Mean error	4.1e-3	6.3e-3	-4.4e-2	-1.2e-2
RMS error	8.0e-2	7.4e-2	8.0e-2	1.5e-1

TABLE IV
LINEARITY CHECK (IN MILLIMETERS)

Direction	*A priori*	implicit 12	inverse 12	inverse 31
1	1.3	0.5	0.49	0.59
2	2.3	0.49	0.58	1.1

[2]The experimental results turned out to be insensitive to the selection of the 71-pose set.

[3]Exhaustive results, not given for sake of clarity, can be found in [36].

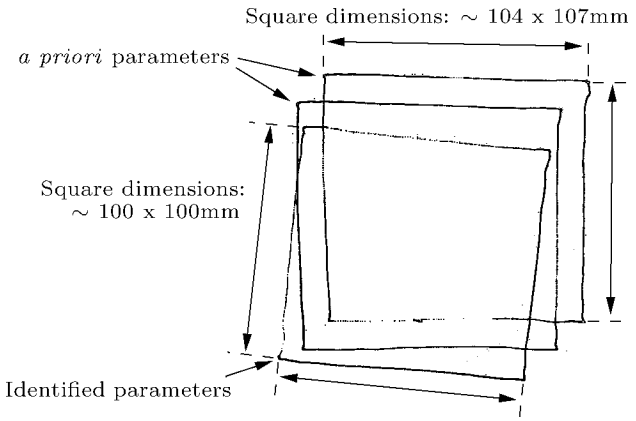

Fig. 8. Comparison of graphically recorded end-effector trajectories.

Notice also that using the *a priori* parameters rather than the identified ones yields a noticeable approximate positioning error of the nacelle of 26 mm and 1.3°.

The influence of the calibration method is presented before discussing the optimal calibration model.

Implicit/Inverse Model: For the two models, the kinematic parameter variations are significant w.r.t. the *a priori* values with length modification of several millimeters, and variation of the angles defining the joint positions and joint offsets on the order of two degrees (Table II). The residual errors are sharply reduced in both cases, and the linearity check improved. Since the two models contain the same information about the kinematics of the end-effector, the influence of the model is only due to its numerical properties. In this case, no significant difference is observed. The linearity check is only slightly improved by the use of the implicit model (Table IV). The latter, which can be derived for any parallel mechanism, seems therefore the more adequate for the calibration.

Calibration Model Influence: The linearity check shows a lower efficiency of the 31-model by comparison with the inverse or implicit 12-model (Table IV). For further analysis of this efficiency decrease, other identifications have been achieved with the 12- and 31-models, taking into account *a priori* information on the kinematic parameters. Eight variants have been finally evaluated, with 10–31 kinematic parameters to identify (Table V).

For each case, the condition number of the identification Jacobian matrix and mean linearity check are indicated in Table VI.

Mean and RMS errors, not indicated for sake of clarity, are constantly decreasing with the model complexity increase. They do not seem to be significant indicators of the calibration efficiency, since linearity check variation (Table VI) is not consistent with the latter.

According to the linearity check indicator, the models based on the 31-model seem to be less efficient than those built from the 12-model. For the vision-based measuring device, models based on the 12-model are the most efficient, and one can here observe the existence of the optimal calibration model, as stated in [49].

In Table II, one may notice that the most important length variation for the 12-model (variant D) is the forearm length

TABLE V
IDENTIFIED MODELS WITH *A PRIORI* INFORMATION ADDED TO REFERENCE MODEL

Model	Reference model	Nb. of kinem. param.	*a priori* information added to the reference model
A	12	10	Nacelle dimension h Forearm length l
B	12	11	Nacelle dimension h
C	12	11	Forearm length l
D	12	12	-
E	31	23	Identical arm lengths L Nacelle dimension h Forearm length l
F	31	26	Nacelle dimension h Forearm length l
G	31	27	Forearm length l
H	31	31	-

TABLE VI
CONDITION NUMBER OF IDENTIFICATION JACOBIAN MATRIX, MEAN LINEARITY CHECK FOR MODELS DEFINED INTABLE V

	A	B	C	D
Condition number	115	160	116	161
Linearity check (mm)	0.61	0.54	0.62	0.55
	E	F	G	H
Condition number	187	192	194	220
Linearity check (mm)	0.79	0.88	0.88	0.77

L, with a modification of about 7 mm. This 7-mm modification seems rather huge, compared with the *a priori* knowledge on this dimension. Introducing this *a priori* knowledge, however, reduces the calibration efficiency, with better results using models B, D, H, than with A, C, G (Table VI). Furthermore, introduction of the forearm length as a parameter to identify significantly increases the condition number.

These results seem to be justified by further analysis of the mechanism kinematic behavior. The variation of the nacelle orientation axis has been measured in the order of 0.1°. This variation is due to the nonrespect of the assumption concerning the forearm geometry. Identifying their equivalent length probably enables us to compensate for the model error. A complete modeling of the parallelograms could be achieved, according to Visher [11]. However, the associated parameters seem rather difficult to identify, and we did not include such a modeling.

Finally, the optimal calibration model using the proposed vision-based calibration method seems to be the model issued from the CAD hypotheses. An efficient compromise is probably then obtained between the number of parameters to identify, and their influence on the kinematic model, as measured with the proposed vision-based measuring device. Such an observation has also been obtained for the Orthoglide mechanism [41] with an approximately equal workspace ($300\times300\times300$ mm^3).

V. CONCLUSION – DISCUSSION

In this paper, we proposed a comprehensive method for parallel mechanism kinematic calibration using vision-based metrology. To do so, we introduced a novel camera-plus-target calibration method. Making explicit the relative positions of the camera and the target with respect to the mechanism in the

kinematic calibration algorithm (either based on the inverse or the implicit kinematic model), we exhibited three classes of potentially nonidentifiable parameters: nonidentifiable kinematic parameters, nonidentifiable external parameters, and coupled kinematic and external parameters.

Extensive experimental results have shown the efficiency of vision-based kinematic calibration procedures. The accuracy of the introduced vision-based measuring device has been evaluated on the order of 10 μm in position, and $5e-4^{\circ}$ in orientation. The accuracy of an existing robot has then been improved by a factor of 10 according to three different validation procedures. Using the full-pose measurement provided by the vision-based measuring device, analysis of the kinematic behavior of the mechanism has also been achieved, with selection of the optimal calibration model.

The presented results show that our simple and automated calibration procedure, achievable in less than one hour on the mechanism, enables us to calibrate a parallel robot, with final accuracy less than 1 mm when using a standard video camera. The implicit model calibration and the use of the design model are sufficient to get such an accuracy, which tends to indicate that the proposed procedure can be applied to many parallel structures. This experimental result has been confirmed by calibrating another parallel mechanism with a workspace of same size.

The proposed vision-based measuring device enables us to get a displacement accuracy on the order of 1/100 000 of the measuring volume with now-available cameras. The presented vision-based method therefore fulfills the calibration requirements of parallel robots dedicated to manipulation, with workspace on the order of 1 m^3 and accuracy of 1 mm. Other robots with higher accuracy in a smaller workspace can also be handled, since vision is only sensitive to their ratio. In this context, our method is flexible and enables a full-pose estimation, which has been shown as essential for the selection of the calibration model. Such a method therefore has strong advantages over calibration algorithms based on mechanical constraints or mechanical measuring devices. Vision can also be preferred to laser-based measuring devices for the calibration of parallel manipulators, since our measuring device is of low cost and sufficient accuracy for these mechanisms.

Vision-based calibration is, therefore, a widely applicable solution, dedicated to parallel manipulators, which is complementary to laser-based sensors, more adequate for the calibration of high-accuracy parallel mechanisms such as machine tools.

ACKNOWLEDGMENT

The authors would like to thank all the people who were involved in this work: G. Gogu at LaRAMA, P. Martinet at LASMEA, and F. Pierrot, F. Marquet, and O. Company at LIRMM.

REFERENCES

[1] J.-P. Merlet, *Parallel Robots*. Norwell, MA: Kluwer, 2000.

[2] J. Wang and O. Masory, "On the accuracy of a Stewart platform—Part I : The effect of manufacturing tolerances," in *IEEE Int. Conf. Robot. Autom.*, Atlanta, GA, 1993, pp. 114–120.

[3] W. Khalil and S. Besnard, "Self calibration of Stewart–Gough parallel robots without extra sensors," *IEEE Trans. Robot. Autom.*, vol. 15, no. 6, pp. 1116–1121, Dec. 1999.

[4] D. Daney, "Self calibration of Gough platform using leg mobility constraints," in *Proc. World Congr. Theory Mach. Mech.*, Oulu, Finland, 1999, pp. 104–109.

[5] S. Besnard and W. Khalil, "Identifiable parameters for parallel robots kinematic calibration," in *Proc. IEEE Int. Conf. Robot. Autom.*, Seoul, Korea, 2001, pp. 2859–2866.

[6] L. Baron and J. Angeles, "The on-line direct kinematics of parallel manipulators under joint-sensor redundancy," in *Proc. Adv. Robot Kinematics*, Strobl, Austria, 1998, pp. 126–137.

[7] C. Wampler and T. Arai, "Calibration of robots having kinematic closed loops using nonlinear least-squares estimation," in *Proc. IFTOMM World Congr. Mech. Mach. Sci.*, Nagoya, Japan, Sep. 1992, pp. 153–158.

[8] H. Zhuang, "Self-calibration of parallel mechanisms with a case study on Stewart platforms," *IEEE Trans. Robot. Autom.*, vol. 13, no. 3, pp. 387–397, Jun. 1997.

[9] W. Khalil and D. Murareci, "Autonomous calibration of parallel robots," in *Proc. 5th IFAC Symp. Robot Control*, Nantes, France, 1997, pp. 425–428.

[10] O. Masory, J. Wang, and H. Zhuang, "On the accuracy of a Stewart platform—Part II: Kinematic calibration and compensation," in *Proc. Int. Conf. Robot. Autom.*, Atlanta, GA, 1993, pp. 725–731.

[11] P. Visher, "Improve the accuracy of parallel robot," Ph.D. dissertation, Ecole Polytechnique Fédérale de Lausanne, Lausanne, Switzerland, 1996.

[12] H. Ota, T. Shibukawa, T. Tooyama, and M. Uchiyama, "Forward kinematic calibration method for parallel mechanism using pose data measured by a double ball bar system," in *Proc. Parallel Kinematic Mach. Int. Conf.*, Ann Arbor, MI, Sep. 2000, pp. 57–62.

[13] H. Zhuang, O. Masory, and J. Yan, "Kinematic calibration of a Stewart platform using pose measurements obtained by a single theodolite," in *Proc. Int. Conf. Intell. Robots Syst.*, Pittsburgh, PA, 1995, pp. 329–334.

[14] H. Zhuang, J. Yan, and O. Masory, "Calibration of Stewart platforms and other parallel manipulators by minimizing inverse kinematic residuals," *J. Robot. Syst.*, vol. 15, no. 7, pp. 395–405, 1998.

[15] Y. Koseki, T. Arai, K. Sugimoto, T. Takatuji, and M. Goto, "Design and accuracy evaluation of high-speed and high-precision parallel mechanism," in *Proc. Int. Conf. Robot. Autom.*, Leuven, Belgium, 1998, pp. 1340–1345.

[16] M. Vincze, J. P. Prenninger, and H. Gander, "A laser tracking system to measure position and orientation of robot end-effectors under motion," *Int. J. Robot. Res.*, vol. 13, no. 4, pp. 305–314, 1994.

[17] Z. J. Geng and L. S. Haynes, "A "3-2-1" kinematic configuration of a Stewart platform and its application to six degrees of freedom pose measurements," *Robot. Comput.-Integr. Manuf.*, vol. 11, no. 1, pp. 23–34, 1994.

[18] J. W. Jeong, S. H. Kim, and Y. K. Kwak, "Kinematics and workspace analysis of a parallel wire mechanism for measuring a robot pose," *Mech. Mach. Theory*, vol. 34, no. 6, pp. 825–841, 1999.

[19] H. Zhuang and Z. S. Roth, *Camera-Aided Robot Calibration*. Boca Raton, FL: CRC Press, 1996.

[20] H. G. Maas, "Dynamic photogrammetric calibration of industrial robots," in *Proc. of SPIE Videometrics V* , 1997, pp. 106–112.

[21] J. M. S. T. Motta, G. C. de Carvalho, and R. S. McMaster, "Robot calibration using a 3D vision-based measurement system with a single camera," *Robot. Comput.-Integr. Manuf.*, vol. 17, no. 6, pp. 487–497, 2001.

[22] H. Zou and L. Notash, "Discussions on the camera-aided calibration of parallel manipulators," in *Proc. CCToMM Symp. Mech., Mach., Mechatron.*, Saint-Hubert, QC, Canada, 2001, [CD-ROM].

[23] S. Bai and M. Y. Teo, "Kinematic calibration and pose measurement of a medical parallel manipulator by optical position sensors," *J. Robot. Syst.*, vol. 20, no. 4, pp. 201–209, 2003.

[24] C. W. Wampler, J. M. Hollerbach, and T. Arai, "An implicit loop method for kinematic calibration and its application to closed-chain mechanisms," *IEEE Trans. Robot. Autom.*, vol. 11, no. 5, pp. 710–724, Oct. 1995.

[25] F. Pierrot, F. Marquet, O. Company, and T. Gil, "H4 parallel robot: Modeling, design and preliminary experiments," in *Proc. IEEE Int. Conf. Robot. Autom.*, Seoul, Korea, 2001, pp. 3256–3261.

[26] M. Li and J. M. Lavest, "Some aspects of zoom lens calibration," *IEEE Trans. Pattern Recog. Mach. Intell.*, vol. 18, no. 11, pp. 1105–1110, Nov. 1996.

[27] L. de Agapito, E. Hayman, and I. Reid, "Self-calibration of rotating and zooming cameras," *Int. J. Comput. Vis.*, vol. 2, no. 45, pp. 107–127, 2001.

[28] D. C. Brown, "Close-range camera calibration," *Photogrammetric Eng.*, vol. 8, no. 37, pp. 855–866, 1971.
[29] R. Y. Tsai, "A versatile camera calibration technique for high-accuracy 3D machine vision metrology using off-the-shelf TV cameras and lenses," *IEEE J. Robot. Autom.*, vol. RA-3, no. 4, pp. 323–344, Aug. 1987.
[30] O. Faugeras and G. Toscani, "Camera calibration for 3D computer vision," in *Proc. Int. Conf. Comput. Vis. Pattern Recog.*, Tokyo, Japan, 1987, pp. 25–34.
[31] J. M. Lavest, M. Viala, and M. Dhome, "Do we really need an accurate calibration pattern to achieve a reliable camera calibration?," in *Proc. Eur. Conf. Comput. Vis.*, Freiburg, Germany, 1998, pp. 158–174.
[32] W. Triggs, P. McLauchlan, R. Hartley, and A. Fitzgibbon, *Bundle Adjustment: A Modern Synthesis*, W. Triggs, A. Zisserman, and R. Szeliski, Eds. New York: Springer-Verlag, 2000, Lecture Notes in Computer Science.
[33] *Manual of Photogrammetry*, 4th ed., Amer. Soc. for Photogrammetry and Remote Sensing, Bethesda, MD, 1984.
[34] P. Brand and R. Mohr, "Accuracy in image mesure," in *Proc. SPIE Conf. Videometrics III*, vol. 2350, Boston, MA, 1994, pp. 218–228.
[35] D. F. Dementhon and L. S. Davis, "Model-based object pose in 25 lines of code," *Int. J. Comput. Vis.*, vol. 15, no. 2, pp. 123–141, 1995.
[36] P. Renaud, "Apport de la Vision Pour L'identification Géométrique de Mécanismes Parallèles," Ph.D. dissertation, Univ. Blaise Pascal, Clermont-Ferrand, France, 2003.
[37] W. Khalil and E. Dombre, *Modeling, Identification and Control of Robots*. New York: Taylor & Francis, 2002.
[38] M. Gautier and W. Khalil, "Exciting trajectories for the identification of base inertial parameters of robots," *Int. J. Robot. Res.*, vol. 11, no. 4, pp. 362–375, 1992.
[39] J. Swevers, C. Ganseman, B. D. Tükel, J. De Schutter, and H. Van Brussel, "Optimal robot excitation and identification," *IEEE Trans. Robot. Autom.*, vol. 13, no. 5, pp. 730–740, Nov. 1997.
[40] A. Nahvi and J. M. Hollerbach, "The noise amplification index for optimal pose selection in robot calibration," in *Proc. IEEE Int. Conf. Robot. Autom.*, Minneapolis, MN, 1996, pp. 647–654.
[41] P. Renaud, N. Andreff, G. Gogu, and M. Dhome, "Optimal pose selection for vision-based kinematic calibration of parallel mechanisms," in *Proc. IEEE/RSJ Int. Conf. Intell. Robots Syst.*, Las Vegas, NV, Oct. 2003, pp. 2223–2228.
[42] D. Daney, "Optimal measurement configurations for Gough platform calibration," in *Proc. IEEE Int. Conf. Robot. Autom.*, Washington, DC, 2002, pp. 147–152.
[43] W. Khalil, M. Gautier, and C. Enguehard, "Identifiable parameters and optimum configurations for robot calibration," *Robotica*, vol. 9, pp. 63–70, 1991.
[44] M. A. Meggiolaro and S. Dubowsky, "An analytical method to eliminate the redundant parameters in robot calibration," in *Proc. IEEE Int. Conf. Robot. Autom.*, San Francisco, CA, 2000, pp. 3609–3615.
[45] B. Espiau, F. Chaumette, and G. Rives, "A new approach to visual servoing in robotics," *IEEE Trans. Robot. Autom.*, vol. 8, no. 3, pp. 313–326, Jun. 1992.
[46] E. Cervera and Ph. Martinet. Tutorial on advanced visual servoing. presented at *IEEE/RSJ Int. Conf. Intell. Robots Syst.*. [Online]. Available: http://www.robot.uji.es/EURON/visualservoing/tutorial
[47] N. Andreff, P. Renaud, P. Martinet, and F. Pierrot, "Vision-based kinematic calibration of a H4 parallel mechanism: Practical accuracies," *Ind. Robot*, vol. 31, no. 3, pp. 273–283, 2004.
[48] N. Andreff, R. Horaud, and B. Espiau, "Robot hand-eye calibration using structure-from-motion," *Int. J. Robot. Res.*, vol. 20, no. 3, pp. 228–248, 2001.
[49] K. Schroer, "Robot calibration," in *Theory of Kinematic Modeling and Numerical Procedures for Robot Calibration*, R. Bernhardt and S. L. Albright, Eds. London, U.K.: Chapman & Hall, 1993, pp. 157–196.

Pierre Renaud received the Ph.D. degree in 2003 in mechanical engineering from the Blaise Pascal University, Clermont-Ferrand, France.

From 2000 to 2003 he was an Assistant Lecturer with IFMA, Clermont-Ferrand, France. After a postdoctoral position with LIRMM, Monpellier, France, he is now an Associate Professor with INSA Strasbourg, Strasbourg, France. His current research interests are in the field of identification of parallel mechanisms using computer vision and medical robotics.

Nicolas Andreff received the Engineer degree in 1994 from ENSEEIHT, Toulouse, France, spending one year as an Erasmus student in the Automatic Control Department, Lund, Sweden. He received the Ph.D. in 1999 in computer graphics, computer vision and robotics from INPG, Grenoble, France, doing his research at INRIA.

Since 2000, he has been an Associate Professor with IFMA, Clermont-Ferrand, France. His current research interests are in the field of modeling, identification, and control of mechanisms using computer vision.

Jean-Marc Lavest received the Ph.D. degree in computer vision in 1992, after completing an engineering degree in electronics.

He spent one year in Sweden at the Royal Institute of Technology. He then joined the Artificial Vision Research Group "GRAVIR" of LASMEA (UMR 6602 CNRS), Aubière, France, in 1992, and has been the Co-Manager of GRAVIR since 2003. In 2002, he was Research Director for the French companies Vision-IQ and DO-labs. His research interests are perception, sensor modeling, optics, and metrology.

Michel Dhome received the Engineer degree in 1981 from the Ecole Nationale Supérieure des Mines et Techniques Industrielles d'Alès, Alès, France, and the Ph.D. degree from Blaise Pascal University, Clermont-Ferrand, France, in 1984.

He spent the 1984–1985 year as a Postdoctoral Fellow of the Canadian Government at the National Research Council, Ottawa, ON. He is currently a Senior Researcher of the CNRS, attached to the LASMEA laboratory, Aubière, France. His research interests include artificial vision, 3-D object localization, recognition, and modeling.